Discover Oncology

Research

Study on the molecular mechanism of UBA52 and BARD1 regulating hepatocellular carcinoma through the PI3 K/AKT signaling pathway

Chenrui Yang[1] · Yanzhong Zhang[1] · Yajuan Liu[2] · Xiaoyong Wu[1] · Fangyuan Sun[1]

Received: 9 February 2025 / Accepted: 6 May 2025
Published online: 21 May 2025

Abstract

Background Hepatocellular carcinoma (HCC) is one of the leading causes of cancer-related deaths globally, with its development closely related to complex molecular mechanisms such as gene mutations and abnormal signaling pathways. However, the specific roles of many key genes remain unclear. UBA52 and BARD1 are important genes associated with protein degradation, DNA repair, and cell cycle regulation, but their mechanisms in liver cancer are not well understood.
Methods This study integrated HCC datasets (GSE135631, GSE184733, GSE202853) from the gene expression omnibus (GEO) database to screen for differentially expressed genes (DEGs), perform functional enrichment analysis, weighted gene co-expression network analysis (WGCNA), construct protein–protein interaction (PPI) networks, and conduct survival analysis. Western Blot (WB) and RT-qPCR experiments were used to verify the expression of UBA52 and BARD1 in liver cancer cells and their association with the PI3K/AKT signaling pathway.
Results Bioinformatics analysis identified UBA52 and BARD1 as core genes, showing high expression in HCC tissues and correlation with poor prognosis. Western Blot and RT-qPCR results further confirmed the high expression of UBA52 and BARD1 in HCC cell lines (HepG2 and Hep3b). PI3K inhibitors significantly downregulated the expression of UBA52 and BARD1, restored the levels of apoptosis-related factors (Fas, BAX, Caspase-3), and inhibited the expression of cell cycle-related proteins (Cyclin-D1, c-Myc). These findings suggest that UBA52 and BARD1 may regulate HCC cell proliferation, apoptosis, and metastasis through the PI3K/AKT signaling pathway. Furthermore, the molecular mechanism of hepatocellular carcinoma can be modulated by knocking out BARD1 or UBA52.
Conclusion UBA52 and BARD1 are highly expressed in HCC, and their abnormal expression may promote the occurrence and development of liver cancer by regulating the PI3K/AKT signaling pathway and mechanisms related to apoptosis and cell cycle. The high expression of UBA52 and BARD1 is closely associated with poor prognosis, indicating their potential value as early diagnostic and targeted therapeutic biomarkers for HCC.

Keywords Hepatocellular carcinoma · UBA52 · BARD1 · PI3 K/AKT signaling pathway · Differentially expressed genes · Bioinformatics · Apoptosis

Supplementary Information The online version contains supplementary material available at https://doi.org/10.1007/s12672-025-02600-5.

✉ Yanzhong Zhang, zyz01011966@126.com; Chenrui Yang, rui15235538728@163.com; Yajuan Liu, 648458453@qq.com; Xiaoyong Wu, 15035150329@163.com; Fangyuan Sun, sunfangyuanoo@126.com | [1]Department of General Surgery, Danzhou People's Hospital (Danzhou People's Hospital Medical Group), 21-1 Datong Road, Nada Town, Danzhou City 571700, Hainan, China. [2]Department of Clinical Pharmacy, Danzhou People's Hospital (Danzhou People's Hospital Medical Group), 21-1 Datong Road, Nada Town, Danzhou City 571700, Hainan, China.

Abbreviations

HCC	Hepatocellular carcinoma
GEO	Gene expression omnibus
WGCNA	Weighted gene co-expression network analysis
PPI	Protein–protein interaction
WB	Western Blot
DEGs	Differentially expressed genes
FC	Fold change
FDR	False discovery rate
MAD	Median Absolute Deviation
TOM	Topological Overlap Matrix
GO	Gene Ontology
KEGG	Kyoto Encyclopedia of Genes and Genomes
GSEA	Gene Set Enrichment Analysis
STRING	Search Tool for the Retrieval of Interacting Genes
CTD	Comparative Toxicogenomics Database

1 Introduction

Hepatocellular carcinoma (HCC) is the predominant form of liver cancer (accounting for 75–85%), and it ranks as the third leading cause of cancer-related deaths globally, following lung cancer and colorectal cancer. In 2022, the number of deaths from liver cancer worldwide had exceeded 750,000 cases, with the incidence and mortality rates in males being 2 to 3 times higher than those in females [1]. The occurrence of liver cancer is usually closely related to high-risk factors such as chronic hepatitis virus (HBV or HCV) infection, liver cirrhosis, alcohol abuse, and metabolic syndrome [2, 3]. However, the pathogenesis of many cases remains not fully understood, which makes it particularly important to explore the molecular basis of liver cancer, early diagnostic biomarkers, and therapeutic targets.

The molecular mechanisms of liver cancer involve multiple aspects, including gene mutations, chromosomal abnormalities, epigenetic modifications, and dysregulation of signaling pathways [4–6]. Genomic sequencing studies have identified that key gene mutations, such as those in CTNNB1, TP53, and AXIN1, as well as abnormalities in signaling pathways like Wnt/β-catenin, PI3 K/AKT/mTOR, and TGF-β, play important roles in liver cancer [7–9]. These studies have provided a theoretical basis for the mechanisms underlying the development of liver cancer. However, many unknown genes and pathways still require further investigation. Abnormal regulation of gene expression may promote the occurrence and development of cancer by affecting mechanisms such as cell proliferation, apoptosis, and immune evasion.

In recent years, bioinformatics technologies have been widely used in the study of disease molecular mechanisms by integrating genomics, transcriptomics, and proteomics data [10]. By using methods such as differentially expressed genes (DEGs) analysis, enrichment analysis, and signaling pathway analysis, researchers can efficiently identify key genes related to diseases and explore their potential molecular mechanisms. Particularly in the field of tumor genomics, bioinformatics technologies have promoted the precise development of cancer diagnosis and treatment research.

UBA52 and BARD1 are two important genes associated with cell cycle regulation, DNA repair, and protein degradation, and they are abnormally expressed in a variety of malignant tumors. UBA52 encodes a ubiquitin-ribosome fusion protein that is involved in protein degradation and cell cycle regulation. BARD1, as a binding protein of BRCA1, maintains genomic stability through DNA repair and cell cycle regulation [11, 12]. Previous studies have indicated that these genes may be involved in the development of cancer by regulating key signaling pathways (such as PI3 K/AKT and Wnt/β-catenin), but their specific mechanisms in liver cancer remain unclear.

Therefore, this paper combines bioinformatics analysis and experimental validation to systematically study the expression patterns and biological functions of UBA52 and BARD1 in liver cancer. Through enrichment analysis and pathway analysis, we explore whether these two genes affect the occurrence and development of liver cancer through specific mechanisms and verify their potential value in the diagnosis and targeted treatment of liver cancer.

2 Methods

2.1 HCC datasets

In this study, the HCC datasets GSE135631, GSE184733, and GSE202853, which were generated from GPL16791, GPL24676, GPL11154, and GPL21290, were downloaded from the gene expression omnibus (GEO) database (http://www.ncbi.nlm.nih.gov/geo/). The GSE135631 dataset includes 15 HCC and 15 normal tissue samples, the GSE184733 dataset includes 17 HCC and 17 normal tissue samples, and the GSE202853 dataset includes 10 HCC and 10 normal tissue samples. These datasets were used to identify differentially expressed genes (DEGs) in HCC.

2.2 Batch effect removal

For the merging and batch effect removal of multiple datasets, we first used the R package to merge the datasets GSE135631, GSE184733, and GSE202853. Specifically, the R package inSilicoMerging [DOD:https://doi.org/10.1186/1471-2105-13-335] was employed to merge these datasets, resulting in a combined matrix. Subsequently, the removeBatchEffect function from the R package limma (version 3.42.2) was utilized to eliminate batch effects. The final matrix, free of batch effects, was then applied to subsequent analyses.

2.3 Identification of DEGs

The R package "limma" was used for summarizing probes and background correction of the combined matrix of GSE135631, GSE184733, and GSE202853. The Benjamini–Hochberg method was employed to adjust the raw p-values. Fold change (FC) was calculated using the false discovery rate (FDR). The cutoff criteria for DEGs were set at $p < 0.05$ and $FC > 1.5$. Volcano plots were generated to visualize and obtain the DEGs.

2.4 Weighted gene co-expression network analysis (WGCNA)

Initially, we utilized the gene expression matrices of GSE135631, GSE184733, and GSE202853 to calculate the Median Absolute Deviation (MAD) for each gene. The genes with the lowest 50% of MAD values were removed. The goodSamplesGenes function from the R package WGCNA was then employed to eliminate outlier genes and samples. Subsequently, a scale-free co-expression network was constructed using WGCNA. Specifically, a Pearson correlation matrix and average linkage hierarchical clustering were performed for all gene pairs. A weighted adjacency matrix was then constructed using the power function $Amn = |Cmn|^{\beta}$ (where Cmn represents the Pearson correlation between Gene_m and Gene_n, and Amn represents the adjacency between Gene_m and Gene_n). The parameter β is a soft threshold that emphasizes strong correlations between genes while reducing the impact of weak and negative correlations. The adjacency matrix was transformed into a Topological Overlap Matrix (TOM), which measures the network connectivity of a gene, defined as the sum of its adjacencies to all other genes. The corresponding dissimilarity (1-TOM) was also calculated. To classify genes with similar expression profiles into gene modules, average linkage hierarchical clustering was performed based on the TOM-based dissimilarity measure, with a minimum module size of 30 genes. The sensitivity was set to 3. To further analyze the modules, we calculated the dissimilarity of module eigengenes, selected a cutting line for the module dendrogram, and merged some modules. Additionally, modules with a distance less than 0.25 were merged. Notably, the grey module represents the collection of genes that could not be assigned to any module.

Based on the module eigenvalues, the correlation between the module eigenvalues and the phenotype of interest was analyzed, and the module with high correlation with the phenotype (large absolute value) was selected as the key module. Modules with an absolute value of correlation greater than 0.2 or 0.3 May be potentially associated with the phenotype. Module size is also an important consideration. Modules that are too small may be unstable or lack biological significance, and a lower limit on the number of genes within the module is generally set. Gene significance is the correlation between gene expression and phenotype. In WGCNA, GS values were obtained by calculating the Pearson correlation coefficient between each gene and phenotype, which ranged from − 1 to 1. Genes with an absolute value

of GS greater than a certain threshold were selected as genes significantly associated with the phenotype. Common thresholds are set at 0.2, 0.3, or higher, and a P value of less than 0.05 is used to further determine the threshold.

2.5 Functional enrichment analysis

Gene Ontology (GO) and Kyoto Encyclopedia of Genes and Genomes (KEGG) analyses are computational methods for evaluating gene functions and biological pathways. In this study, the list of differentially expressed genes (DEGs) filtered by Venn diagram was input into the KEGG REST API (https://www.kegg.jp/kegg/rest/keggapi.html) to obtain the latest KEGG Pathway gene annotations, which served as the background. The genes were mapped to this background set, and the R package clusterProfiler (version 3.14.3) was used to perform enrichment analysis to obtain the results of gene set enrichment. Additionally, the GO annotations of genes from the R package org.Hs.eg.db (version 3.1.0) were used as the background, and the genes were mapped to this background set. The minimum gene set size was set to 5, and the maximum gene set size was set to 5000. A p-value of < 0.05 and a FDR of < 0.25 were considered statistically significant measures.

Furthermore, the Metascape database provides comprehensive gene list annotation and analysis resources with visualization and export capabilities. We used the Metascape database (http://metascape.org/gp/index.html) to perform functional enrichment analysis on the aforementioned list of DEGs and export the results.

2.6 Gene set enrichment analysis (GSEA)

For gene set enrichment analysis (GSEA), we obtained the GSEA software (version 3.0) from the GSEA website. The samples were divided into two groups based on disease and normal tissue. We downloaded the c2.cp.kegg.v7.4.symbols.gmt subset from the Molecular Signatures Database to evaluate relevant pathways and molecular mechanisms. Based on gene expression profiles and phenotypic grouping, the minimum gene set size was set to 5, and the maximum gene set size was set to 5000. One thousand permutations were performed. False discovery rate (FDR) is a common method to deal with multiple comparisons in gene set enrichment analysis (GSEA), which adjusts the P value by controlling the false discovery rate. It calculates the expected proportion of false positives among all results considered significant. The FDR threshold was set at 0.05, which allowed up to 5% of all gene sets judged to be significant to be false positives. A p-value < 0.05 was considered statistically significant. Additionally, GO and KEGG analyses were performed on the whole genome as specified by GSEA.

2.7 Immune infiltration analysis

CIBERSORT (http://CIBERSORT.stanford.edu/) is a widely used method for calculating immune cell infiltration. The LM22 gene signature was used to define 22 immune cell subsets. We applied an integrated bioinformatics approach using the CIBERSORT software package to analyze the merged gene expression matrix of the HCC dataset. The expression matrix of immune cell subsets was deconvoluted using the principle of linear support vector regression to estimate the abundance of immune cells. A confidence level of $p < 0.05$ was used as the cutoff criterion to select samples with sufficient confidence.

2.8 Construction and analysis of protein–protein interaction (PPI) network

The Search Tool for the Retrieval of Interacting Genes (STRING) database (http://string-db.org/) aims to collect, score, and integrate all publicly available sources of protein–protein interaction information and supplement these sources with computational predictions. In this study, the list of DEGs was input into the STRING database to construct a PPI network for predicting core genes (confidence > 0.4). Cytoscape software provides biologists with tools for biological network analysis and two-dimensional visualization. In this study, Cytoscape software was used to visualize and predict core genes from the PPI network formed by the STRING database. The PPI network was first imported into Cytoscape. The MCODE algorithm was used to identify the most relevant module. Additionally, the top ten genes with the highest relevance were calculated using five algorithms (MCC, Degree, Closeness, BottleNeck, Radiality), and the intersection was taken. The list of core genes was visualized and exported.

2.9 Survival analysis

Clinical survival data for HCC were obtained from TCGA. The R package maxstat (version: 0.7–25) was used to calculate the best cutoff value of the RiskScore for core genes. The minimum group sample size was set to be greater than 25%, and the maximum group sample size was set to be less than 75%. The best cutoff value was calculated. Based on this, patients were divided into high and low groups. The R package survival's survfit function was used to analyze the prognostic differences between the two groups, and the log-rank test was employed to assess the significance of prognostic differences between different groups.

2.10 Gene expression heatmap

The R package heatmap was used to generate heatmaps of the expression levels of core genes identified in the PPI network in the merged matrix of GSE135631, GSE184733, and GSE202853. The expression differences of core genes between HCC and normal tissue samples were visualized.

2.11 CTD analysis

The Comparative Toxicogenomics Database (CTD) integrates a large amount of interaction data between chemicals, genes, functional phenotypes, and diseases, providing great convenience for research on disease-related environmental exposure factors and potential mechanisms of drug action. The core genes were input into the CTD website to identify the most relevant diseases. Excel was used to create radar charts showing the expression differences of each gene.

2.12 miRNA analysis

TargetScan (http://www.targetscan.org) is an online database for predicting miRNA and target gene interactions. In our study, TargetScan was used to identify miRNAs that regulate the central DEGs.

2.13 Western blot experiment

2.13.1 Cell culture and grouping

Human normal liver cells (L-O2) were used as the control group, while the Hep G2 and Hep3b human HCC cell lines were used as the experimental groups. Cell line source: Search and purchase through the official website of China National Cell Bank. The cells were cultured in high-glucose DMEM medium supplemented with fetal bovine serum and maintained in a 37 °C incubator with 5% CO_2, with regular medium changes. The cells were divided into the following groups: control group (CON group, L-O2 cells), Hep G2 group (Hep G2 cells), Hep3b group (Hep3b cells), Hep G2-PI3 K inhibitor group (PI3 K inhibitor added to Hep G2 cells), and Hep3b-PI3 K inhibitor group (PI3 K inhibitor added to Hep3b cells). Types and concentrations of PI3 K inhibitors: pan-PI3 K inhibitors, which inhibit multiple isoforms of PI3 K simultaneously, with concentrations ranging from 1–100 μmol/L.

2.13.1.1 Protein extraction and quantification Cells were washed 2–3 times with PBS, and an appropriate amount of RIPA lysis buffer containing protease inhibitors was added. The cells were lysed for 3–5 min in the culture plate, then scraped and transferred to a 1.5 mL centrifuge tube. After lysis on ice for 30 min, the samples were centrifuged at 12,000 rpm for 10 min at 4 °C, and the supernatant was collected as the total protein solution. Protein concentration was quantified using a BCA kit (Thermo, ND2000, USA), with a standard curve used to calculate the concentration.

2.13.1.2 SDS-PAGE electrophoresis and transfer Protein samples were mixed with 5 × protein loading buffer at a 1:4 ratio and heated at 99 °C for 10 min before loading. Electrophoresis was performed at 160 V for 40 min. Proteins were trans-

ferred to a pre-treated PVDF membrane under conditions of 400 mA for 25 min. The transfer buffer was prepared as a mixture of anhydrous ethanol and pure water (20:80).

2.13.1.3 Blocking and primary antibody incubation After transfer, the PVDF membrane was blocked in 5% bovine serum albumin at room temperature for 1 h. The following primary antibodies (all diluted at 1:1000) were added: UBA52 (Proteintech, 18039-1-AP), BARD1 (Proteintech, 22964-1-AP), Caspase-3 (Proteintech, 66470-2-Ig), CyclinD1 (Proteintech, 60186-1-Ig), PI3 K (Proteintech, ID= 67071-1-Ig), AKT (Proteintech, 60203-2-Ig). GAPDH was used as the internal reference. The membrane was incubated overnight at 4 °C.

2.13.1.4 Secondary antibody incubation and chemiluminescent detection After removing the primary antibodies, the PVDF membrane was washed three times with TBST (each wash lasting 5–10 min), followed by the addition of secondary antibodies (Goat Anti-Rabbit IgG/HRP or Goat Anti-Mouse IgG/HRP, Solarbio, diluted 1:5000) and incubated at room temperature for 1 h. After washing three times, enhanced chemiluminescent solution (ECL) was added and incubated for 1 min before detection on a chemiluminescent imager. The data were analyzed using AIWBwellTM software.

2.13.2 Cell grouping

Con group; HepG2 group; Hep3b group; HepG2-UBA52_KO group: UBA52 siRNA-transfected HepG2; Hep3b-UBA52_KO group: UBA52 siRNA-transfected Hep3b; HepG2-BARD1_KO group: BARD1 siRNA-transfected HepG2; Hep3b-BARD1_KO group: BARD1 siRNA-transfected Hep3b.

UBA52 siRNA sequence: SS sequence CGACUACAACAUCCAGAAGA, AS sequence UUUCUGGAUGUUGUAGUCGGA.

BARD1 siRNA sequence: SS sequence GGAGAAGAAGGUCUGUGUAAA, AS sequence UACACAGACCUUCUUCUCCGG.

Transfection of UBA52 or BARD1 siRNA into HepG2 and Hep3B cells. Both cell lines were seeded in 6-well plates at specific densities (HepG2: 2×10^5 cells/mL; Hep3B: 1.5×10^5 cells/mL) and cultured for 24 h in their respective media (DMEM with 10% FBS for HepG2; MEM with 10% FBS + 1% NEAA for Hep3B) until reaching 50–60% confluency. The prepared siRNA-transfection reagent complexes were mixed with 125 µL Opti-MEM, incubated for 15 min, then added to cell wells. Complete medium replacement was performed at 6 h (HepG2) or 4 h (Hep3B) post-transfection to reduce cytotoxicity. Cells were harvested 48 h post-transfection for RNA extraction using TRIzol, followed by qPCR validation of knockdown efficiency. Protein was extracted 72 h post-transfection using RIPA lysis buffer (containing protease inhibitors), and protein expression levels were analyzed by Western blot with GAPDH as the loading control.

2.14 PCR experiment

We performed RT-qPCR validation and divided the cells into the following five groups: CON group (normal liver cells L-O2), HepG2 group (HepG2 human HCC cells), Hep3b group (Hep3b human HCC cells), HepG2-PI3 K inhibitor group (PI3 K inhibitor added to HepG2 cells), and Hep3b-PI3 K inhibitor group (PI3 K inhibitor added to Hep3b cells).

First, a cell suspension of 1×10^6 cells was transferred to a 1.5 mL centrifuge tube and centrifuged at $500 \times g$ for 3 min using an Eppendorf centrifuge (model 5810R, Germany) to collect the cell pellet. Subsequently, 500 µL of lysis buffer was added, and the cells were thoroughly lysed by pipetting up and down 10 times and vortexing for 10 s. Then, an equal volume of anhydrous ethanol was added and mixed thoroughly by inverting the tube or pipetting to disperse any precipitates. The mixture was transferred to an RNA extraction column and centrifuged for 1 min to collect the supernatant.

Total RNA was treated with DNase to remove genomic DNA. Specifically, 100 ng to 2 µg of total RNA was mixed with 2 µL of DNase (ES Science, RT001, Shanghai) and RNase-free water to a final volume of 16 µL. The mixture was gently pipetted 5–10 times to mix thoroughly and incubated at 25 °C for 5 min, followed by cooling on ice. The RNA concentration and purity were determined using a NanoDrop 2000 micro-spectrophotometer (Thermo, USA). Subsequently, 4 µL of 5 × RT Mix (ES Science, RT001, Shanghai) was added to each 16 µL RNA sample. The mixture was thoroughly mixed and incubated at 42 °C for 15 min to reverse transcribe the RNA into cDNA. The resulting cDNA samples were diluted 5–10 times and used as templates for qPCR.

The qPCR reaction system was 20 µL, including 10 µL of 2 × SYBR Green qPCR Mix (ES Science, QP002, Shanghai), 0.4 µL of ROX dye, 1–4 µL of diluted cDNA template, 0.4 µL of forward primer (10 µM), and 0.4 µL of reverse primer (10 µM), with ddH_2O added to make up to 20 µL. The qPCR reaction program was set as follows: initial denaturation

at 95 ℃ for 5 min, followed by 40 cycles, each consisting of denaturation at 95 ℃ for 10 s and annealing/extension at 60 ℃ for 30 s. Finally, the melting curve analysis was completed according to the instrument's default settings.

The primer sequences for the target genes are as follows:

BARD1: Forward primer (5'-AAGGAGCCCGTGTGCTTAG'), Reverse primer (5'-TTGCCCTAGATGTGTTGTCTTTT-3').

UBA52: Forward primer (5'-CATCACTCTTGAGGTCGAGCC-3'), Reverse primer (5'-CTTGGGCTGAATTGAAGGTTTTG-3').

GAPDH: Forward primer (5'-GTTTGCCCGCGAATATCAGC-3'), Reverse primer (5'-GGCTGTTGTCATACTTCTCATGG-3').

All experimental data were collected using the StepOneTM Real-Time PCR System and analyzed using the 2^(-ΔΔCT) method. Each experimental group was repeated at least three times, and the data are presented as mean ± standard deviation. Statistical significance was determined by ANOVA ($p < 0.05$).

3 Results

3.1 Differential expression gene analysis

In this study, according to the set cutoff values, we identified differentially expressed genes (DEGs) in the merged matrix of the HCC datasets GSE135631, GSE184733, and GSE202853, resulting in a total of 1277 DEGs (Fig. 1).

3.2 Functional enrichment analysis

3.2.1 Functional enrichment analysis of DEGs

We performed GO and KEGG analyses on these differentially expressed genes. According to the GO analysis results, in BP analysis, they were mainly enriched in mRNA metabolic processes and cell cycle (Fig. 2A). In CC analysis, they were mainly enriched in cytoplasmic parts and cell matrix junctions (Fig. 2B). In MF analysis, they were mainly focused on protein transporter activity and structural molecule activity (Fig. 2C). In KEGG analysis, they were mainly enriched in the PI3 K-Akt signaling pathway, cell cycle, apoptosis, AMPK signaling pathway, and HCC (Fig. 2D).

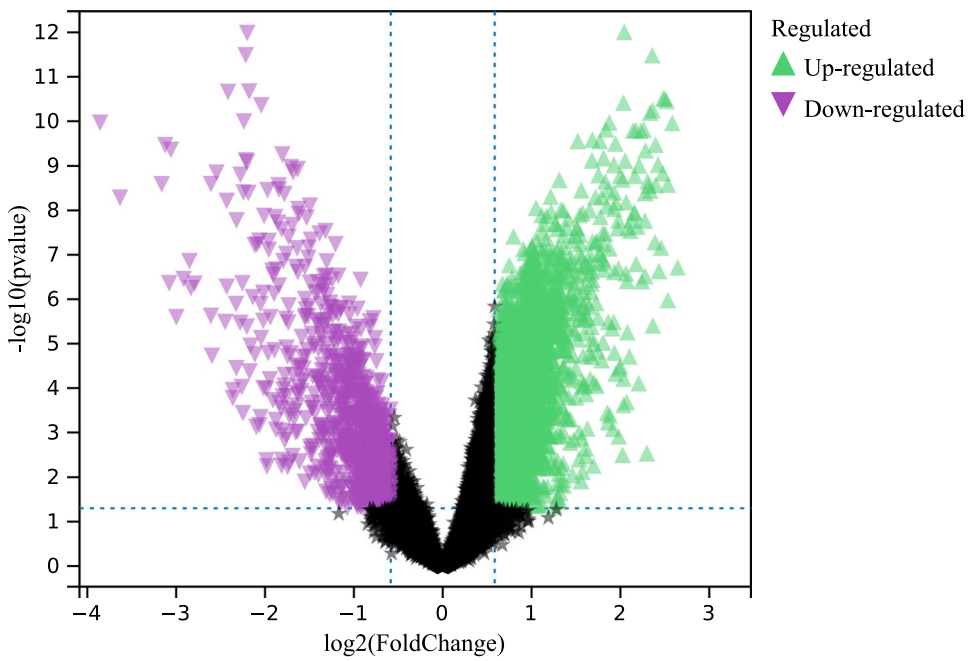

Fig. 1 Differential gene analysis. A total of 1277 DEGs

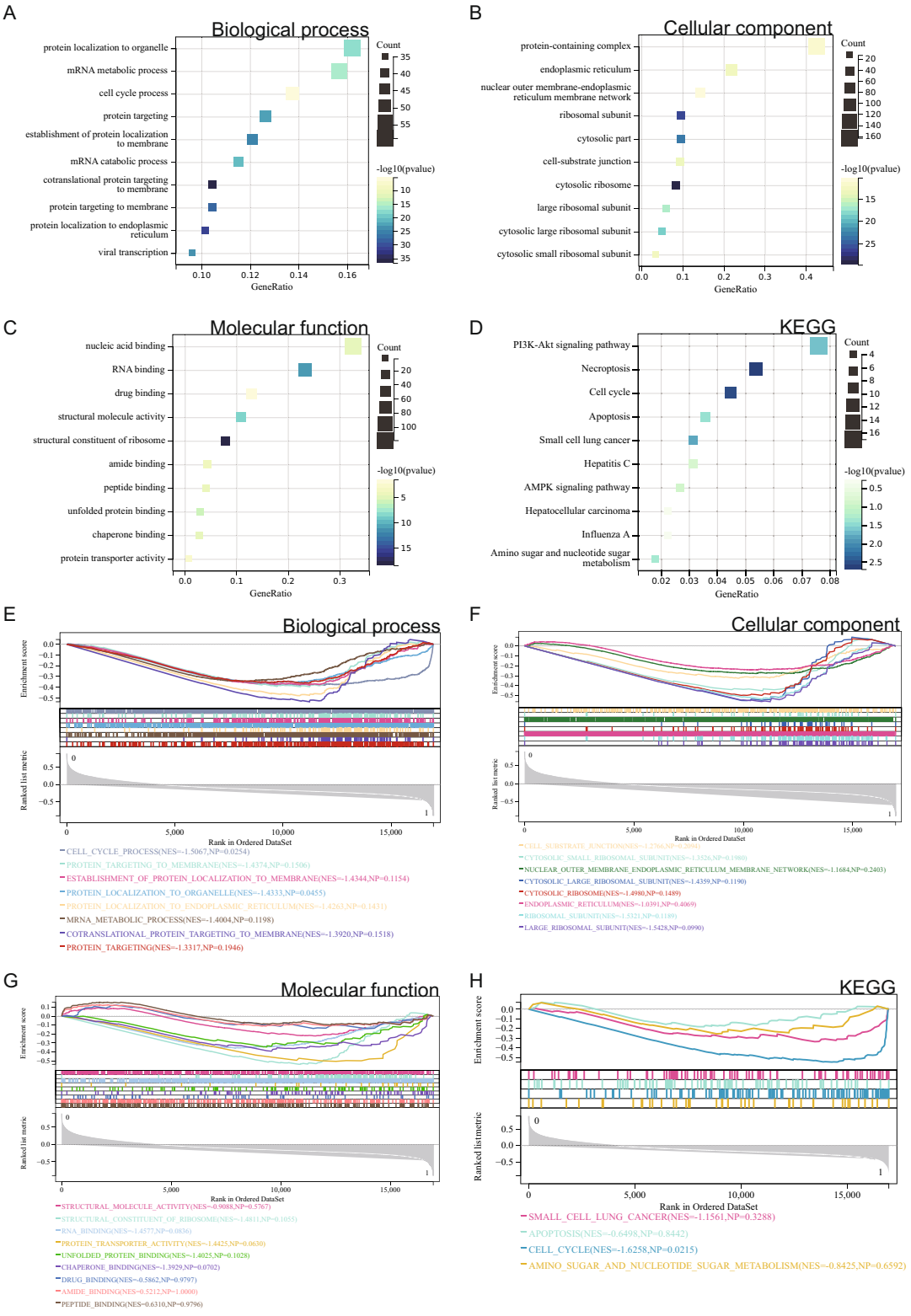

Fig. 2 **A**–**D** Results of GOKEGG enrichment analysis of DEGs. **A** Biological process analysis. **B** Cellular component analysis. **C** Molecular function analysis. **D** KEGG enrichment analysis. **E**–**H** Results of GSEA of DEGs. **E** Biological process analysis. **F** Cellular component analysis. **G** Molecular function analysis. **H** KEGG enrichment analysis

3.2.2 GSEA

Additionally, we performed GSEA on the whole genome to identify potential enrichments among non-differentially expressed genes and to validate the results of differentially expressed genes. The intersection of enrichment terms with the GO KEGG enrichment terms of differentially expressed genes is shown in the figure. The merged matrix enrichment results of the HCC datasets GSE135631, GSE184733, and GSE202853 show that differentially expressed genes are mainly enriched in mRNA metabolic processes, cell cycle, cell matrix junctions, protein transporter activity, cell cycle, and apoptosis (Fig. 2E–H).

3.2.3 Metascape enrichment analysis

In the Metascape enrichment projects, GO enrichment projects revealed genes and protein expressions related to cell cycle, adaptive immune system, JAK-STAT signaling after interleukin-12 stimulation, and TNF-α/NF-kappa B signaling complex (Fig. 3A). We also outputted the enrichment network colored by enrichment terms and p-values (Fig. 3B, C, Fig. 4), visually representing the associations and confidence levels of each enrichment term.

3.3 WGCNA

The selection of soft threshold power is an important step in WGCNA. Network topology analysis was conducted to determine the soft threshold power. The soft threshold power in WGCNA was set to 6 (Fig. 5A). A hierarchical clustering tree of all genes was constructed, and interactions among significant modules were generated and analyzed (Fig. 5B), resulting in a total of 10 modules (Fig. 5C). We also generated a heatmap of module-trait correlations (Fig. 5D) and a scatter plot of GS and MM correlations for related hub genes (Fig. 5E). We also constructed a Venn diagram of the differentially expressed genes screened by WGCNA and DEGs and took the intersection (Fig. 5F).

3.4 Construction and analysis of protein–protein interaction (PPI) network

The PPI network of DEGs was constructed by the STRING online database and analyzed by Cytoscape software (Fig. 6A). Then, five algorithms (MCC, Degree, Closeness, BottleNeck, Radiality) were used to identify hub genes (Fig. 6B–F), and a Venn diagram was made to obtain the union as core genes (Fig. 6G). Finally, we identified two core genes (UBA52, BARD1).

3.5 Survival analysis

We obtained prognostic score correlation diagrams from the survival data of HCC downloaded from TCGA. It can be observed that as the risk score increases, the survival rate of patients decreases significantly. The survival time and survival rate of the low-risk group are significantly higher than those of the high-risk group (Fig. 7A). By visualizing the expression heatmap of core genes in the survival data of HCC, it can be seen that the core genes (BARD1, UBA52) are risk factors, and their expression increases with the risk score (Fig. 7B). The KM survival curve of the risk score was drawn, and it can be seen that the risk score has a significant impact on survival rate (Fig. 7C). We also obtained the survival curves of core genes in HCC patients (Fig. 7D). The results show that the expression of core genes (UBA52, BARD1) is significantly related to survival rate and may play a certain role in the prognosis of HCC patients.

3.6 Core gene expression heatmap

We visualized and made heatmaps of the expression levels of core genes in the merged matrix of HCC datasets GSE135631, GSE184733, and GSE202853 (Fig. 8A). We found that the core genes (UBA52, BARD1) are highly expressed in HCC samples and lowly expressed in normal samples. Based on these results, we speculate that the core genes (UBA52, BARD1) may have a regulatory role in HCC.

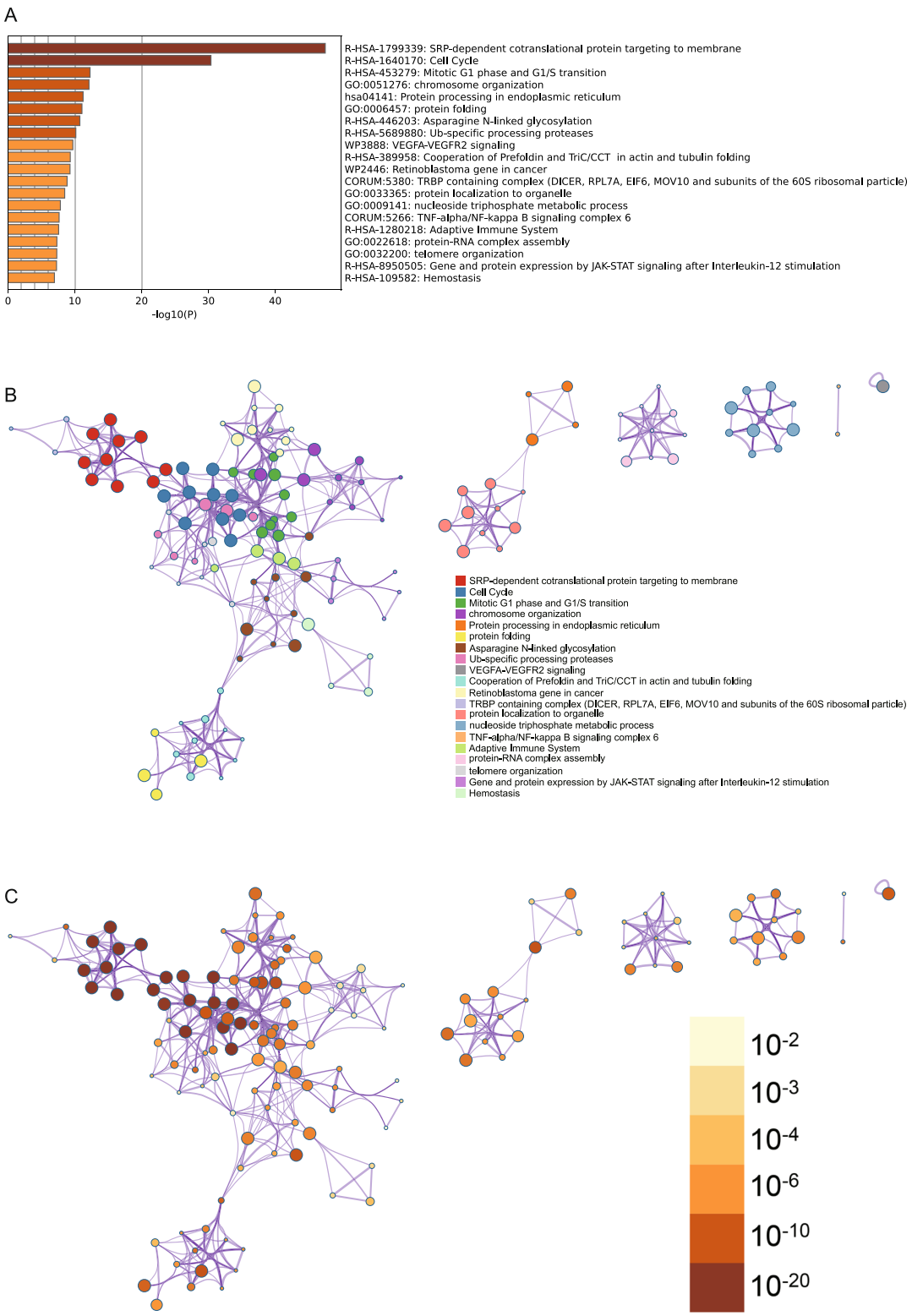

Fig. 3 Metascape enrichment analysis. **A** Bar graph of enriched terms across input gene lists, colored by p-values. **B** Network of enriched terms: colored by cluster ID, where nodes that share the same cluster ID are typically close to each other. **C** Colored by p-value, where terms containing more genes tend to have a more significant p-value

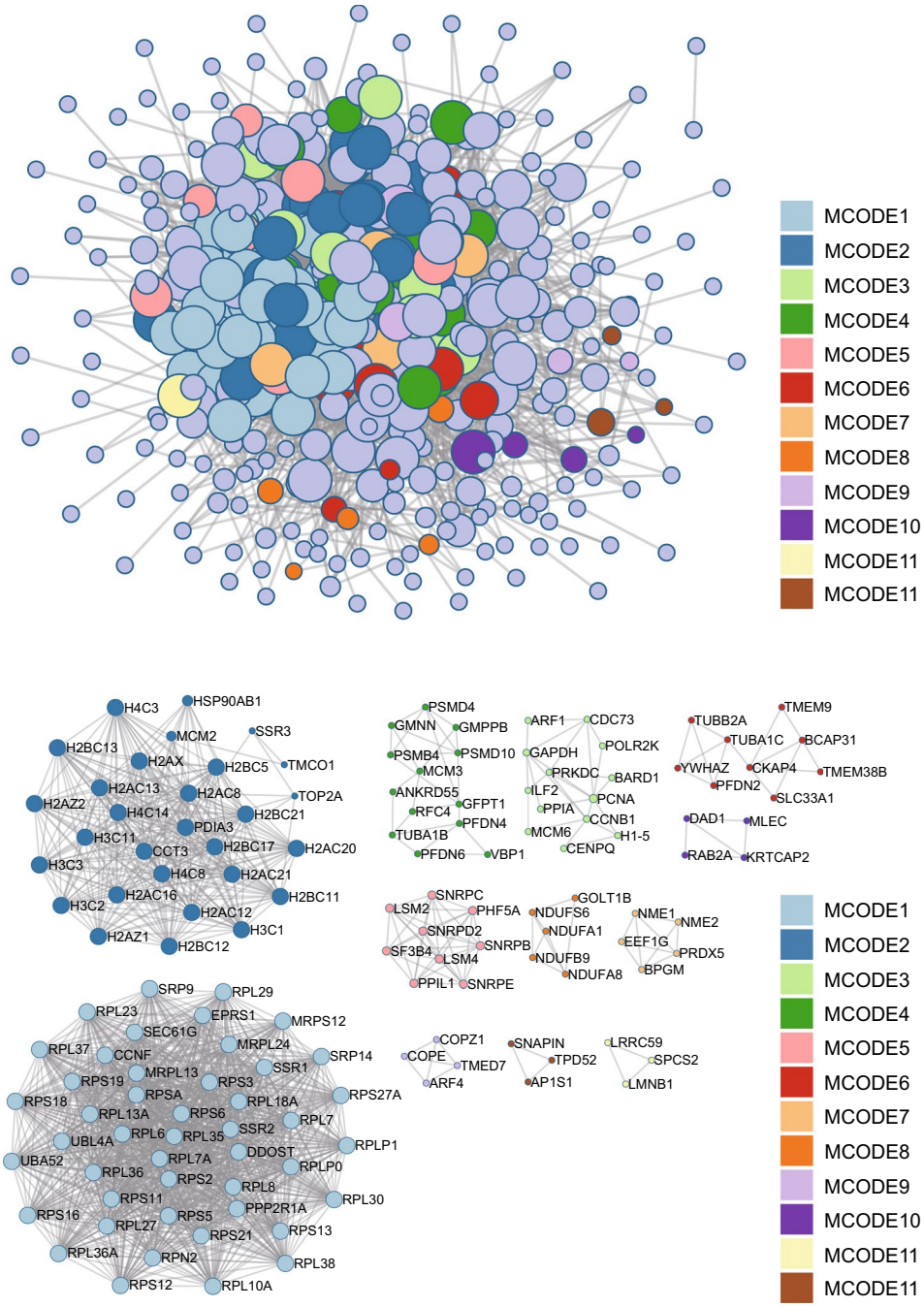

Fig. 4 Protein–protein interaction network. And MCODE components identified in the gene lists

3.7 CTD analysis

In this study, we input the hub gene list into the CTD website to find diseases related to core genes, enhancing the understanding of gene-disease associations. It was found that the core genes (UBA52, BARD1) are associated with liver tumors, liver diseases, cirrhosis, inflammation, and necrosis (Fig. 8B).

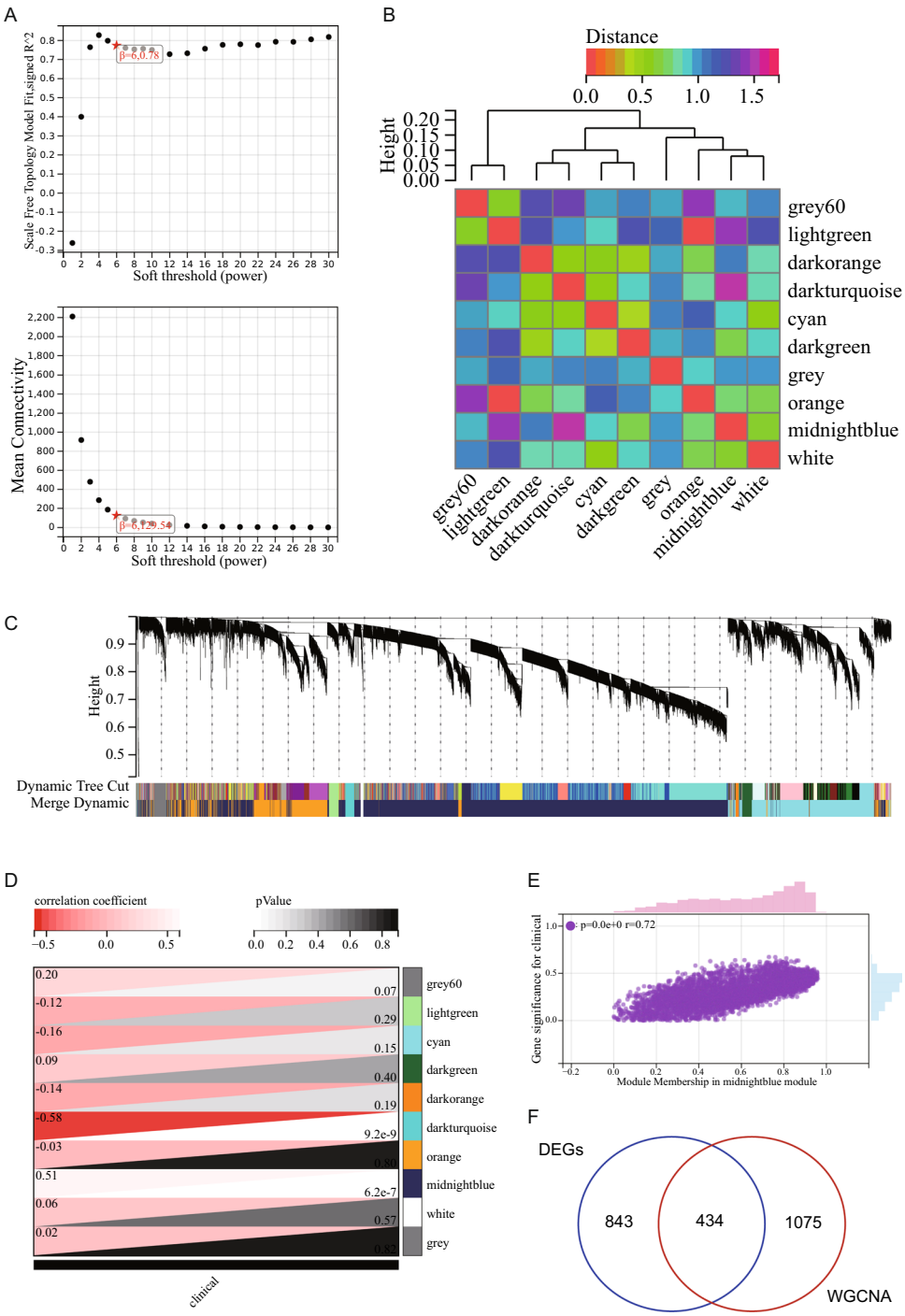

Fig. 5 WGCNA. **A** β = 6,0.78. β = 6,129.54. **B**, **C** The hierarchical clustering tree of all genes was constructed, and 10 important modules were generated. **D** The heat map of correlation between modules and phenotypes. **E** The scatter map of correlation between GS and MM of related hub genes. **F** The DEGs screened by WGCNA and DEGs was used to obtain Venn map. 434 intersection genes were obtained

3.8 miRNA prediction and functional annotation related to hub genes

In this study, we input the hub gene list into TargetScan to find related miRNAs, enhancing the understanding of gene expression regulation. A summary of miRNAs that regulate hub genes (Table 1). We found that the related miRNA for the UBA52 gene is hsa-miR-325-3p, and the related miRNA for the BARD1 gene is hsa-miR-383-5p.1.

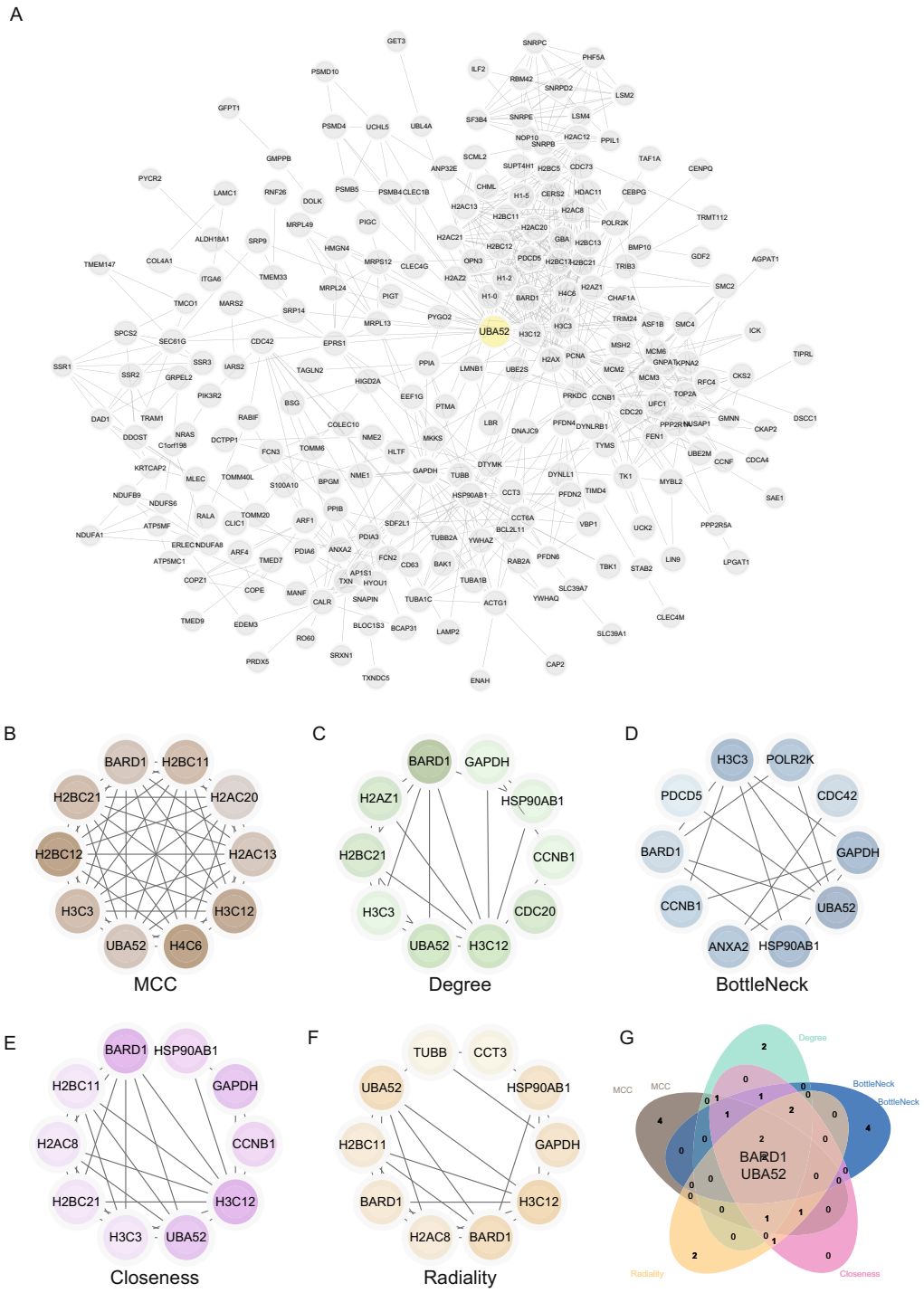

Fig. 6 Construction and analysis of protein–protein interaction (PPI) networks. **A** Construct the PPI network of DEGs using STRING online database and utilize Cytoscape software for analysis. **B** MCC was used to identify the central gene. **C** Degree was used to identify the central gene. **D** BottleNeck was used to identify the central gene. **E** Closeness was used to identify the central gene. **F** Radiality was used to identify the central gene. **G** Core genes (UBA52, BARD1) were obtained by merging using Venn diagrams

3.9 Immune infiltration analysis

We used the CIBERSORT software package to analyze the merged matrix of HCC datasets GSE135631, GSE184733, and GSE202853. At a 95% confidence level, we obtained the proportion of immune cells in the whole gene expression matrix.

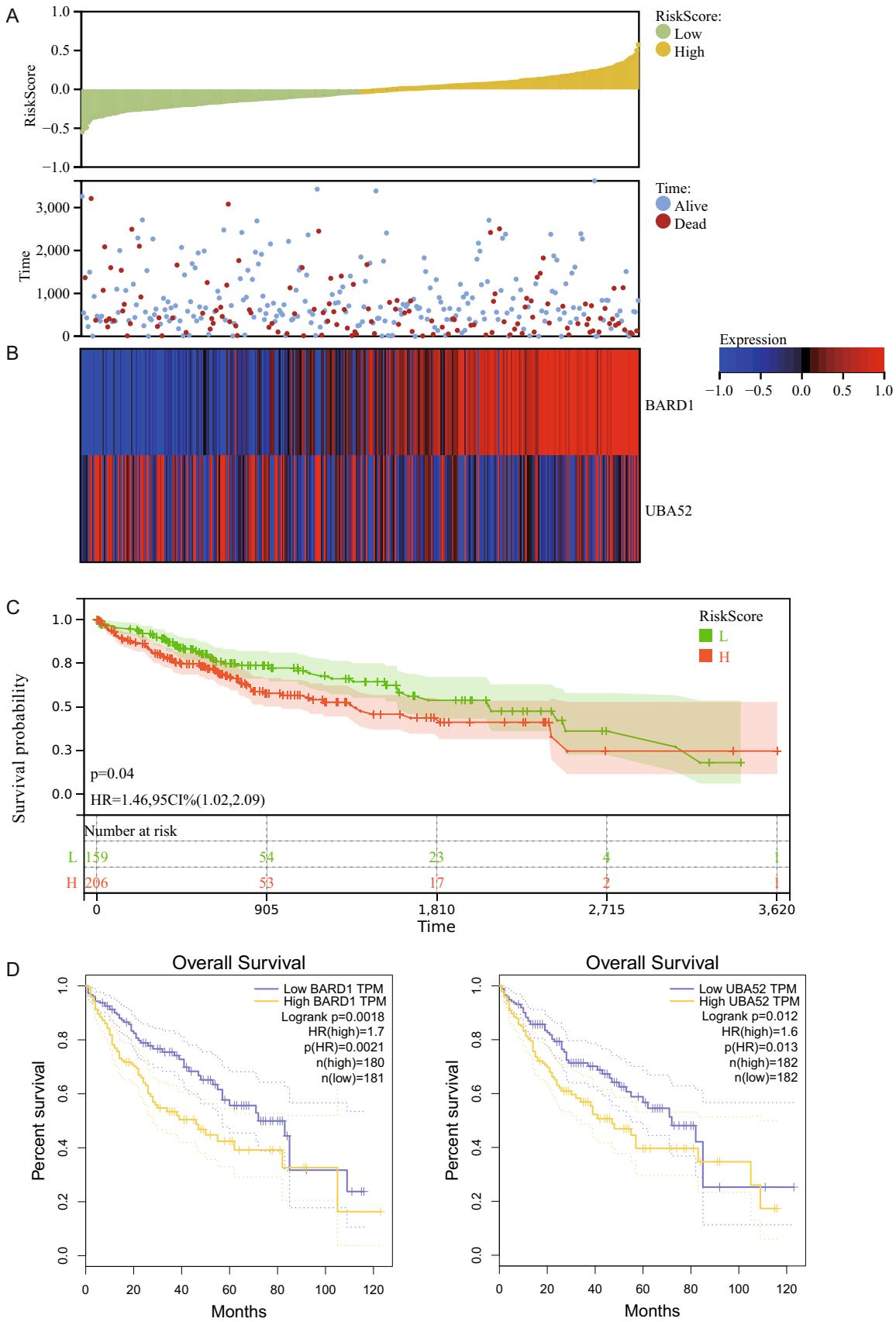

Fig. 7 Prognostic survival analysis. **A** Trend graph of risk score in relation to survival time and survival rate. **B** Expression calorimetric map of core genes in liver cancer survival data. **C** KM survival curve for hazard scores. **D** Overall survival of core genes in patients with liver cancer

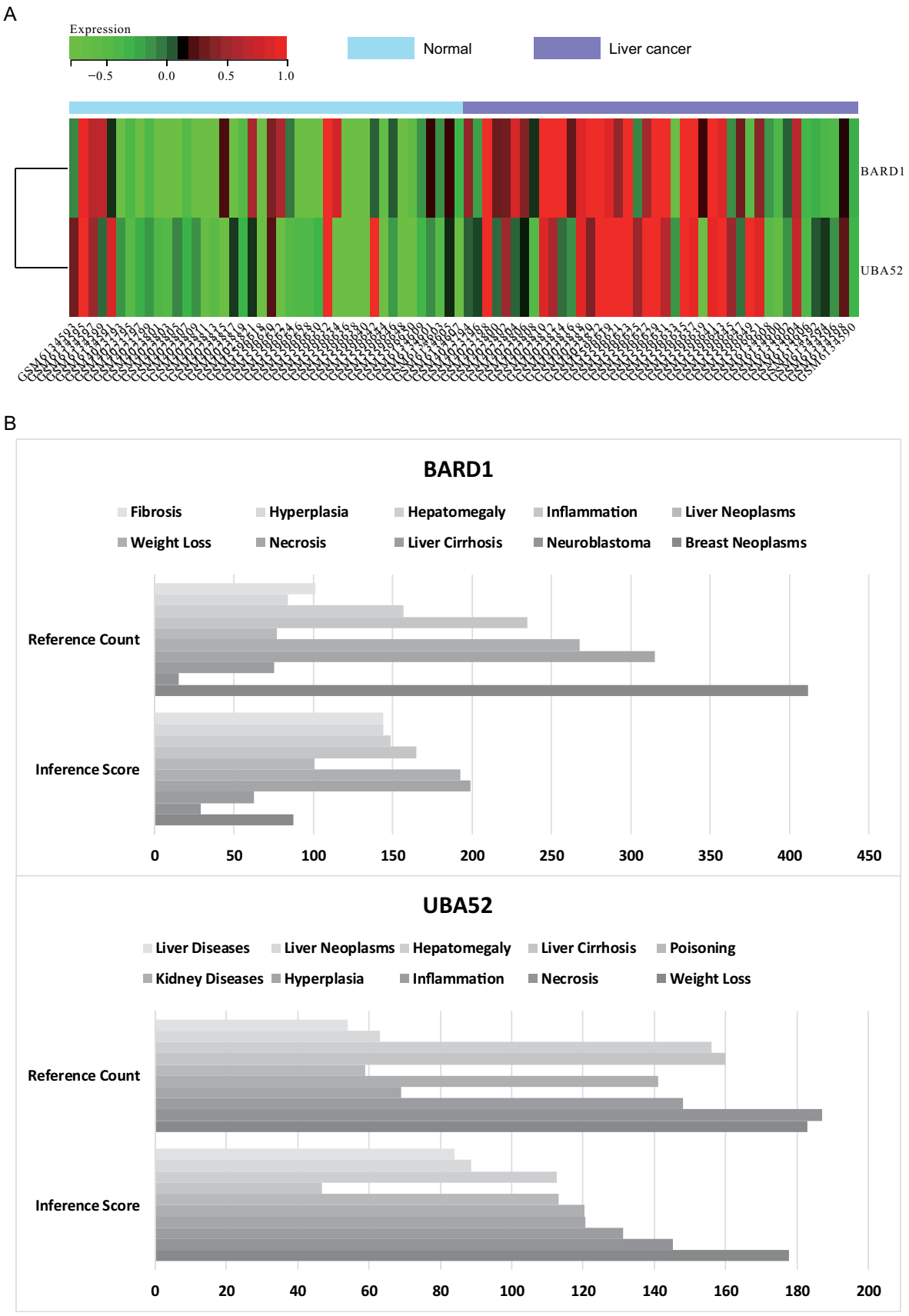

Fig. 8 **A** Heat map of the core gene in the combined matrix of the data sets GSE135631, GSE184733, GSE202853. **B** CTD analysis. Three core genes (UBA52, BARD1) are associated with liver tumors, liver diseases, cirrhosis, inflammation, and necrosis

Table 1 A summary of miRNAs that regulate hub genes

Databases	Gene	miRNA
TargetScan		
	UBA52	hsa-miR-325-3p
	BARD1	hsa-miR-383-5p.1

The results suggest that mast cell activation is relatively high in the samples (Fig. 9A). We also obtained a heatmap of immune cell expression in the dataset (Fig. 9B). Subsequently, we analyzed the correlations of infiltrating immune cells and obtained a co-expression pattern diagram of immune cell components. The results suggest that when activated mast cells are highly expressed, neutrophils are also highly expressed. The positive correlation between activated mast cells and neutrophils may have an impact on the disease process of HCC (Fig. 9C).

3.10 WB experimental analysis of high expression of UBA52 and BARD1 in HCC and signal pathway association

3.10.1 High expression of UBA52 and BARD1 in HCC and association with poor prognosis

WB experimental results show that the expression of UBA52 and BARD1 is low in the normal liver cell group (CON group), but significantly increased in the HCC cell groups (HepG2 group and Hep3b group), with statistical differences compared to the CON group ($p < 0.05$). After the addition of the PI3 K inhibitor, the expression levels of UBA52 and BARD1 in the HepG2-PI3 K inhibitor group and the Hep3b-PI3 K inhibitor group were significantly downregulated. Moreover, the key molecules of the PI3 K/AKT signaling pathway (PI3 K, PIP3, AKT, p-AKT) were upregulated in the HepG2 group and the Hep3b group, but showed a significant downward trend under the action of the PI3 K inhibitor. These results indicate that UBA52 and BARD1 are highly expressed in HCC, and their expression levels are closely related to poor prognosis (Fig. 10).

3.10.2 Downregulation of apoptosis-related protein expression in HCC Cells

Compared with the CON group, the expression of apoptosis-related factors (such as Fas, BAX, P53, Caspase-3, Caspase-9) in the HCC cell groups (HepG2 group and Hep3b group) was significantly downregulated ($p < 0.05$). After the addition of the PI3 K inhibitor, the expression levels of these apoptosis-related factors in the HepG2-PI3 K inhibitor group and the Hep3b-PI3 K inhibitor group were significantly restored ($p < 0.05$). The above results indicate that in HCC cells, the expression of apoptosis proteins is inhibited, and the PI3 K inhibitor can partially reverse this inhibitory effect (Fig. 11).

3.10.3 Upregulation of cell cycle-related protein expression in HCC Cells

Experimental results show that the expression of metastasis-related factors (Cyclin-D1, c-Myc, CDK) in the HCC cell groups (HepG2 group and Hep3b group) was significantly upregulated, while the expression of metastasis-inhibiting factors (P27, RBL2) was downregulated ($p < 0.05$). Under the action of the PI3 K inhibitor, the expression of the above metastasis-related factors in the HepG2-PI3 K inhibitor group and the Hep3b-PI3 K inhibitor group was significantly reduced, and the expression of metastasis-inhibiting factors was significantly increased. These results suggest that the abnormal expression of cell cycle-related proteins in HCC cells may promote tumor cell proliferation and metastasis (Fig. 12).

3.10.4 Western blotting results and bar graph analysis

WB analysis demonstrated that key molecules of the UBA52, BARD1, and PI3 K/AKT signaling pathways (AKT, p-AKT, PI3 K) exhibited low expression levels in normal hepatocytes (L-O2) but were significantly upregulated in hepatocellular carcinoma cells (UBA52, BARD1). In both the UBA52 knockout group and BARD1 knockout group, the expression of these

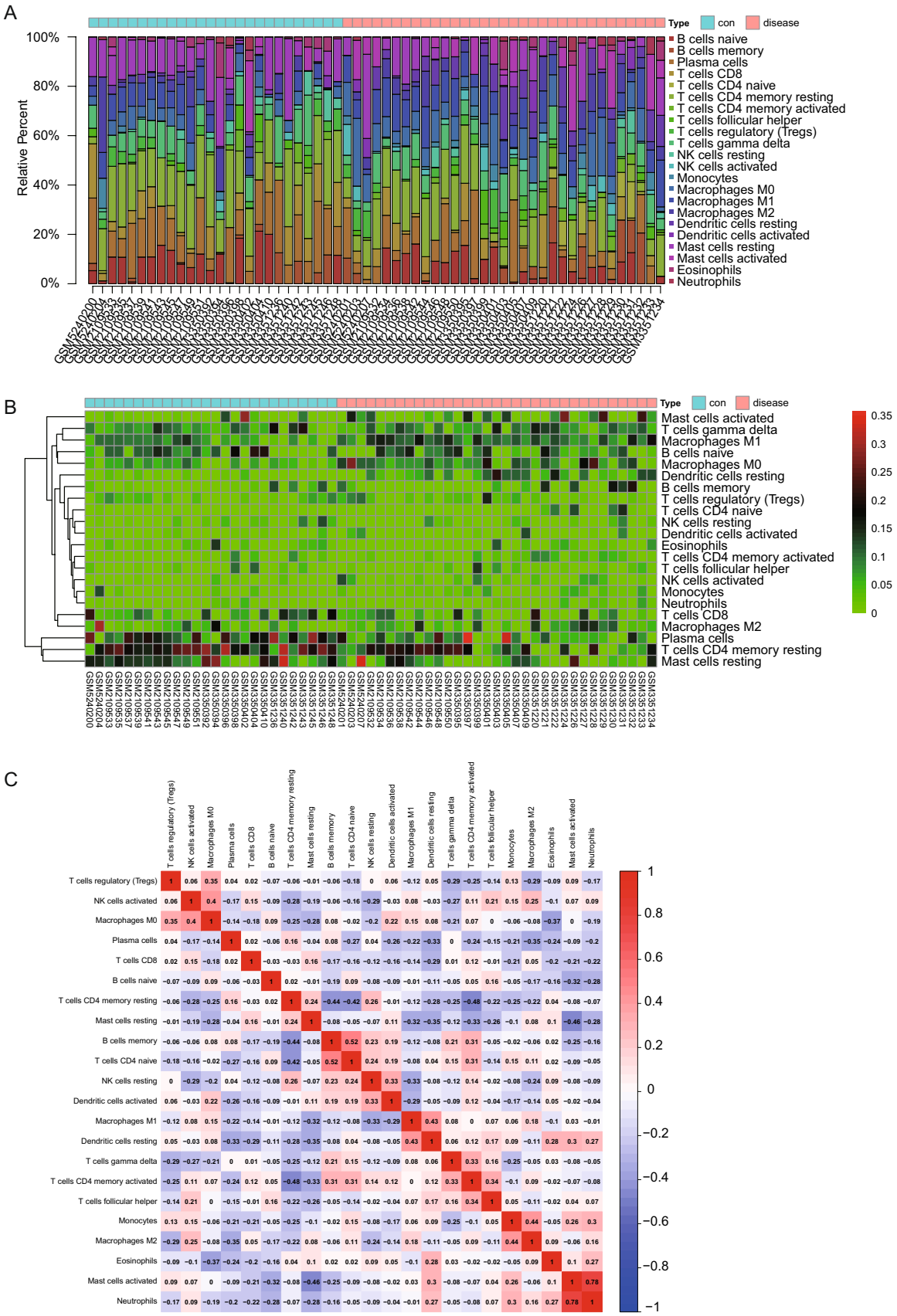

Fig. 9 Immunoinfiltration analysis. **A** Whole gene expression matrix results in proportion of immune cells. **B** Immune cell expression calorigram in a dataset. **C** Map of co-expression patterns between immune cell components

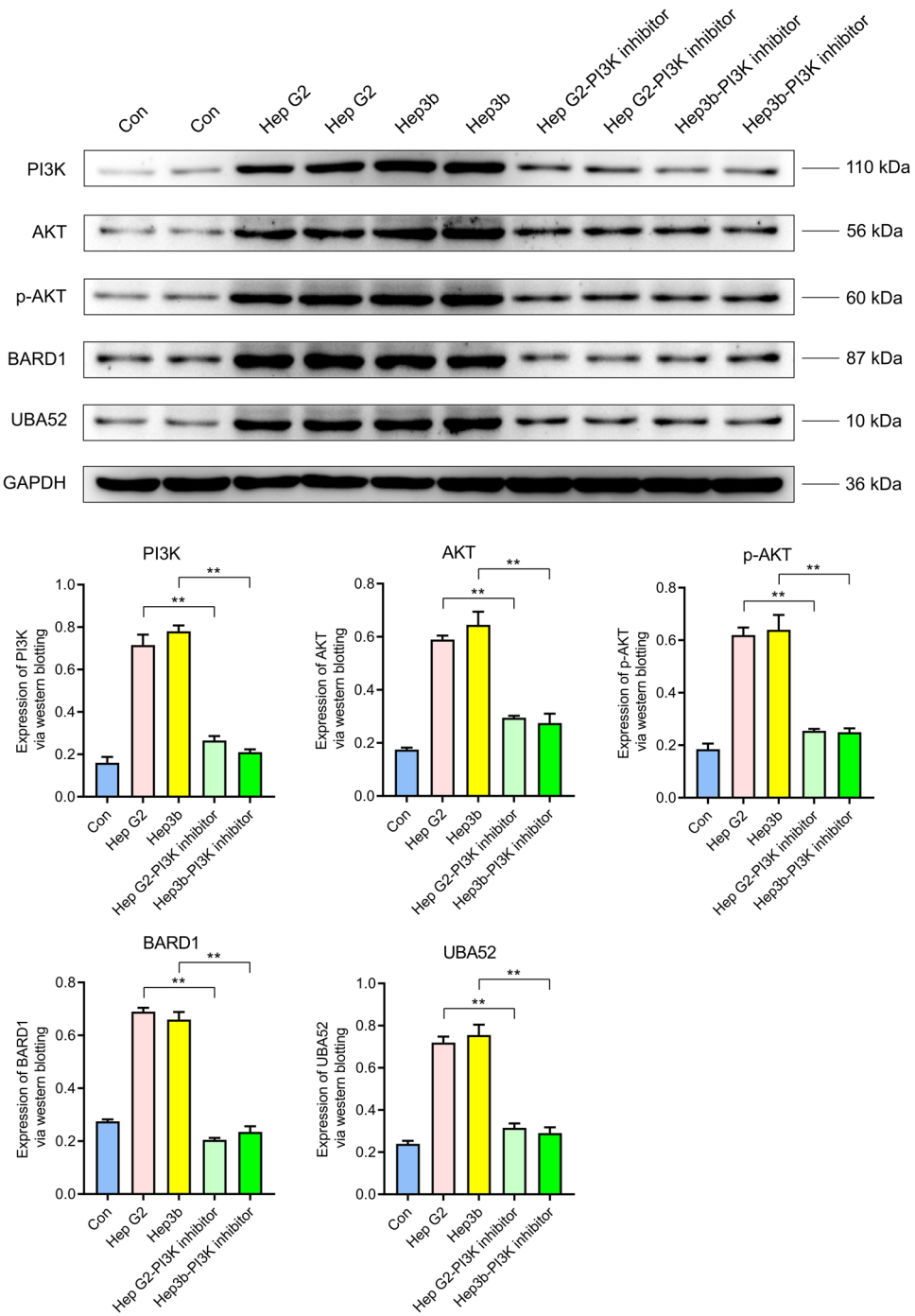

Fig. 10 UBA52 and BARD1 are highly expressed in liver cancer and associated with poor prognosis. Western blot analysis showing significant upregulation of UBA52 and BARD1 in liver cancer cells (HepG2 and Hep3b) compared to normal liver cells (CON group, $p < 0.05$). PI3 K inhibitor treatment reduced the expression of UBA52, BARD1, and PI3 K/AKT pathway-related proteins (PI3 K, PIP3, AKT, p-AKT), indicating their involvement in liver cancer progression

proteins was markedly reduced. Apoptosis- and cell cycle-related regulatory proteins (FAS, Caspase-3, P27) displayed baseline expression in normal hepatocytes (L-O2) but were significantly downregulated in hepatocellular carcinoma cells (UBA52, BARD1). In the UBA52 knockout group and BARD1 knockout group, their protein expression recovered to near-baseline levels. The oncogene c-MYC showed low expression in normal hepatocytes (L-O2) but was highly expressed in hepatocellular carcinoma cells (UBA52, BARD1). In both knockout groups, c-MYC protein expression was significantly downregulated (Figs. 13, 14).

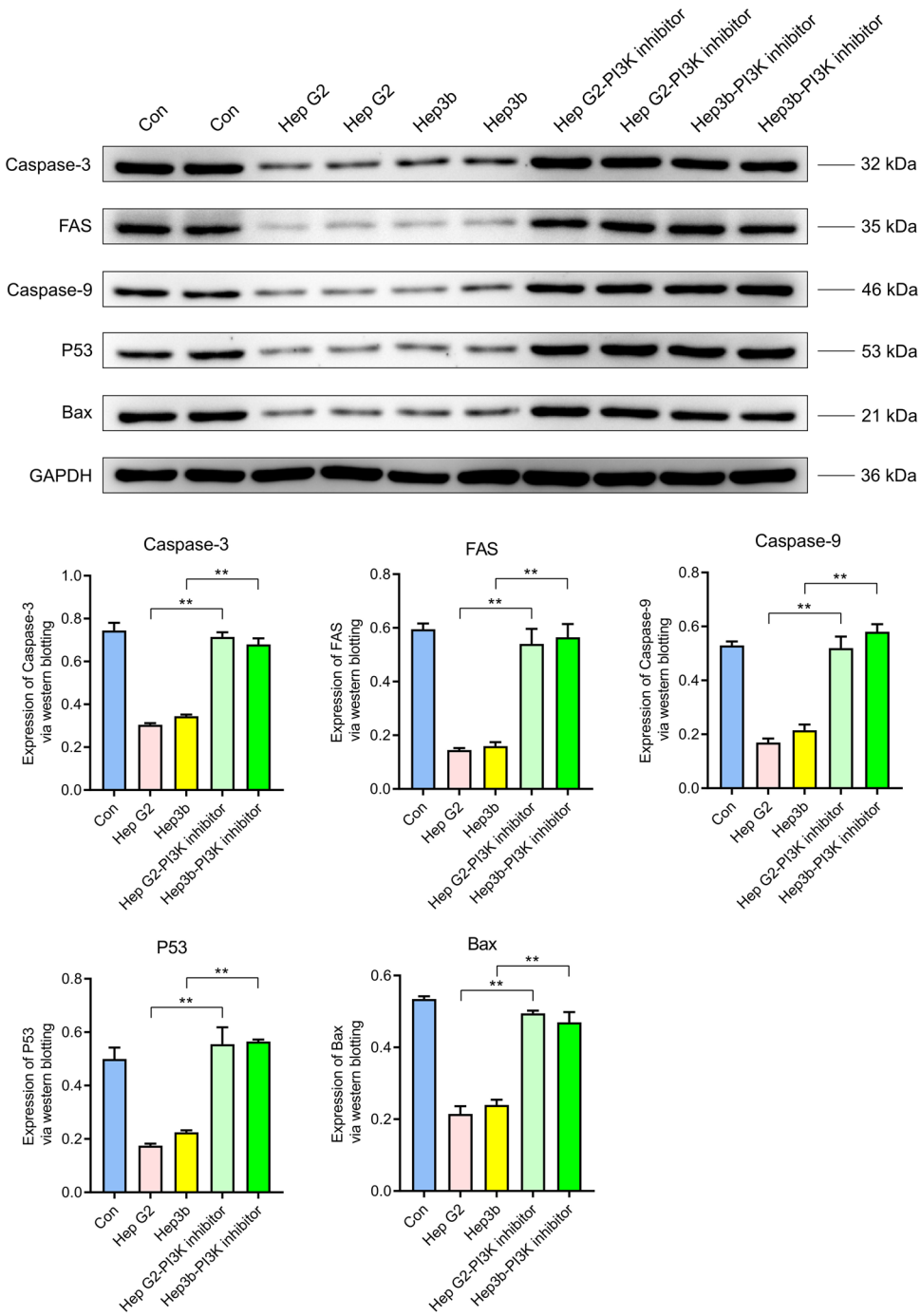

Fig. 11 Apoptosis-related proteins are downregulated in liver cancer cells. Western blot analysis showing reduced expression of apoptosis-related proteins (Fas, BAX, P53, Caspase-3, Caspase-9) in liver cancer cells (HepG2 and Hep3b) compared to normal liver cells (CON group, $p < 0.05$). PI3 K inhibitor treatment restored the expression of these proteins, highlighting the suppression of apoptosis in liver cancer

In summary, BARD1/UBA52 promotes hepatocellular carcinoma (HCC) progression by activating the PI3 K-AKT pathway while suppressing apoptosis-related molecules (FAS/Caspase-3/P27). Knockout of BARD1 or UBA52 reverses these effects and downregulates the oncogene c-MYC.

3.11 RT-qPCR experimental results: expression levels of UBA52 and BARD1 are related to prognosis

RT-qPCR results further verified the high expression of UBA52 and BARD1 in HCC cells. In the normal liver cell group (CON group), the expression levels of UBA52 and BARD1 were low, but significantly increased in the HCC cell groups (HepG2

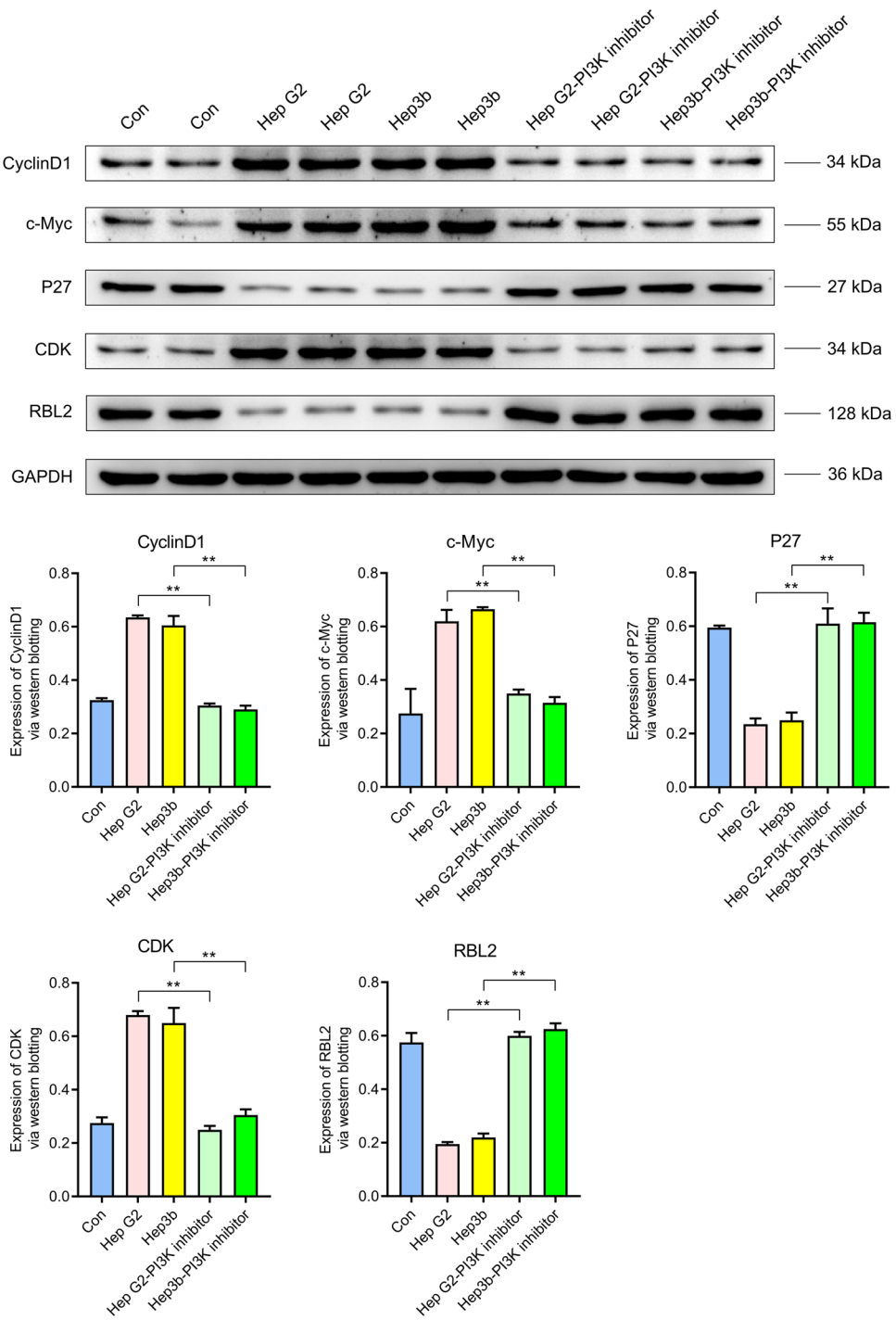

Fig. 12 Cell cycle-related proteins are upregulated in liver cancer cells. Western blot analysis showing increased expression of Cyclin-D1, c-Myc, and CDK, and decreased expression of P27 and RBL2 in liver cancer cells (HepG2 and Hep3b) compared to normal liver cells (CON group, $p < 0.05$). PI3 K inhibitor treatment reversed these changes, suggesting a role for these proteins in promoting liver cancer cell proliferation

group and Hep3b group), with statistical significance compared to the CON group ($p < 0.05$). After the addition of the PI3 K inhibitor, the expression levels of UBA52 and BARD1 in the HepG2-PI3 K inhibitor group and the Hep3b-PI3 K inhibitor group were significantly downregulated ($p < 0.05$). These results indicate that the high expression of UBA52 and BARD1 may be closely related to the occurrence, development, and poor prognosis of HCC (Fig. 15).

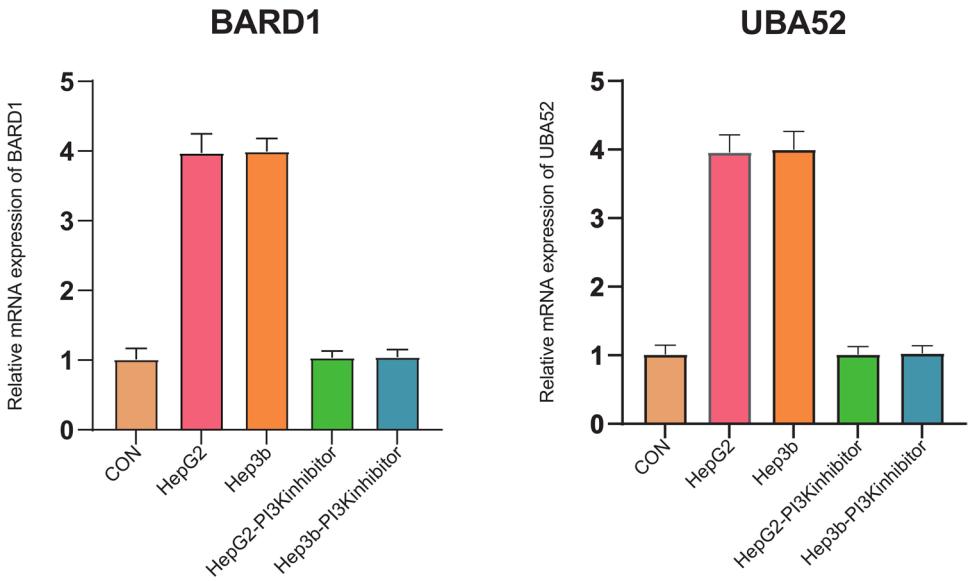

Fig. 13 Western blotting results and bar graph analysis. It presents Western blot detection data on the expression levels of UBA52, BARD1, and key molecules of the PI3 K/AKT signaling pathway (AKT, p-AKT, and PI3 K), along with experimental data following the knockout of UBA52 and BARD1 genes (**** indicates statistically significant differences at $P < 0.0001$)

4 Discussion

HCC is one of the leading causes of cancer-related deaths globally, accounting for the vast majority of liver cancer cases [13]. Despite certain progress in treatment methods including liver resection [14], liver transplantation [15], targeted therapy (such as sorafenib) [16], and immune checkpoint inhibitors [17], the overall therapeutic effect remains limited. Molecular studies have shown that the occurrence of HCC involves abnormal activation of signaling pathways such as Wnt/β-catenin, PI3 K/AKT/mTOR, TGF-β, and VEGF [17–19]. In addition, high-frequency gene mutations (such as CTNNB1, TP53, and AXIN1) play important roles in the occurrence and development of liver cancer by affecting processes such as cell proliferation, differentiation, and apoptosis [20–22]. However, the pathogenesis of liver cancer is complex, and the specific roles of most genes remain to be elucidated.

UBA52 encodes a ubiquitin-ribosome fusion protein and is one of the important genes for maintaining protein homeostasis [23]. As part of the ubiquitin–proteasome system, UBA52 regulates the ubiquitination and degradation of target proteins (such as YAP) by interacting with selenoprotein S, thereby affecting inflammatory responses, cell homeostasis, and signaling pathway activity [24]. Studies have shown that UBA52 plays an important role in cell proliferation and differentiation by regulating protein homeostasis, especially in response to external stimuli and damage [23]. In addition, UBA52 is abnormally expressed in various cancers. For example, in breast cancer, UBA52 is involved in vesicle transport and apoptosis network regulation, affecting cancer cell proliferation and metabolism [25]. In colorectal cancer, UBA52 affects the cell cycle and apoptosis by regulating the RPL40-MDM2-p53 pathway [26]. In multiple myeloma and diffuse large B-cell lymphoma, UBA52 may be involved in disease progression through the PI3 K/AKT and MAPK/ERK signaling pathways [27].

In this study, Western blot and RT-qPCR results showed that UBA52 was significantly overexpressed in HCC cells, and its expression could be downregulated by PI3 K inhibitors, which also restored the levels of apoptosis-related factors such as Fas, BAX, and Caspase-3. These findings are supported by the literature [28]. UBA52 may promote tumor cell proliferation and drug resistance by inhibiting apoptosis.

This study indicates that UBA52 is highly expressed in HCC cells, and PI3 K inhibitors can downregulate the expression of UBA52 as well as molecules related to the PI3 K/AKT signaling pathway. Meanwhile, compared with normal liver cells (CON group), apoptosis-related factors (such as Fas, BAX, and Caspase-3) are significantly downregulated in HCC cells (Hep G2 and Hep3b groups). However, the expression levels of these factors are restored after the addition of PI3 K inhibitors.

BARD1 is a binding protein of BRCA1 that provides E3 ubiquitin ligase activity through its RING domain, participating in DNA repair, cell cycle regulation, and maintenance of genomic stability [29, 30]. BARD1 also regulates the cell cycle and ensures the accuracy of DNA replication by participating in homologous recombination repair and DNA end resection, thereby preventing genomic instability [31]. Abnormal expression of BARD1 has been widely reported in various cancers. In breast and ovarian cancers, its overexpression may promote tumor cell proliferation and invasion through

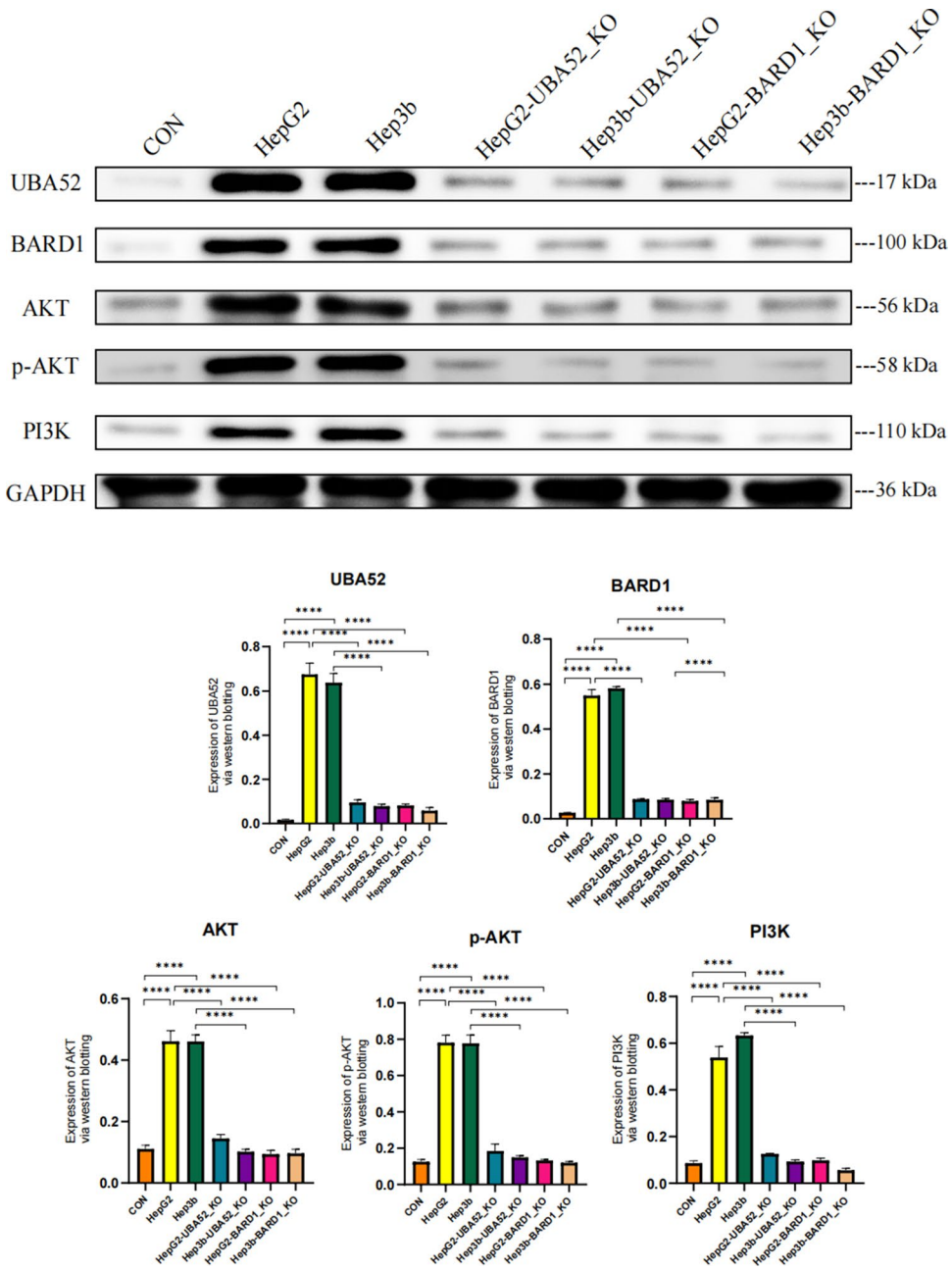

Fig. 14 Western blotting results and bar graph analysis. It presents Western blot data on the expression levels of FAS, Caspase-3, P27, and c-MYC, along with experimental data following UBA52 and BARD1 gene knockout (**** indicates statistically significant differences at $P < 0.0001$)

key roles in transcription and DNA repair [32]. In addition, genetic mutations in BARD1 may lead to DNA repair defects and play a role in cancers such as neuroblastoma [33]. In pancreatic cancer, BARD1, as a target of HuR, is crucial for DNA double-strand break repair and cell cycle regulation. Downregulation of BARD1 leads to G2/M cell cycle arrest, further exacerbating DNA damage [34]. This study shows that BARD1 is highly expressed in the HCC cell lines Hep G2 and Hep3b, and PI3 K inhibitors can effectively downregulate its expression and restore the levels of apoptosis-related factors. This suggests that BARD1 may be involved in the progression of HCC and chemoresistance by regulating apoptosis pathways and the cell cycle, providing a new direction for targeted therapy of HCC.

The relatively higher mast cell activation in HCC samples is significant in the context of UBA52 and BARD1 expression. The protein encoded by UBA52 is involved in the process of ubiquitination, which is closely related to protein degradation and cell cycle regulation. Mast cells can release a variety of cytokines and inflammatory mediators after activation, which may affect the tumor microenvironment. Mast cell activation was relatively high in HCC samples, possibly interacting with UBA52 expression. On the one hand, the normal expression of UBA52 is essential for maintaining intracellular protein

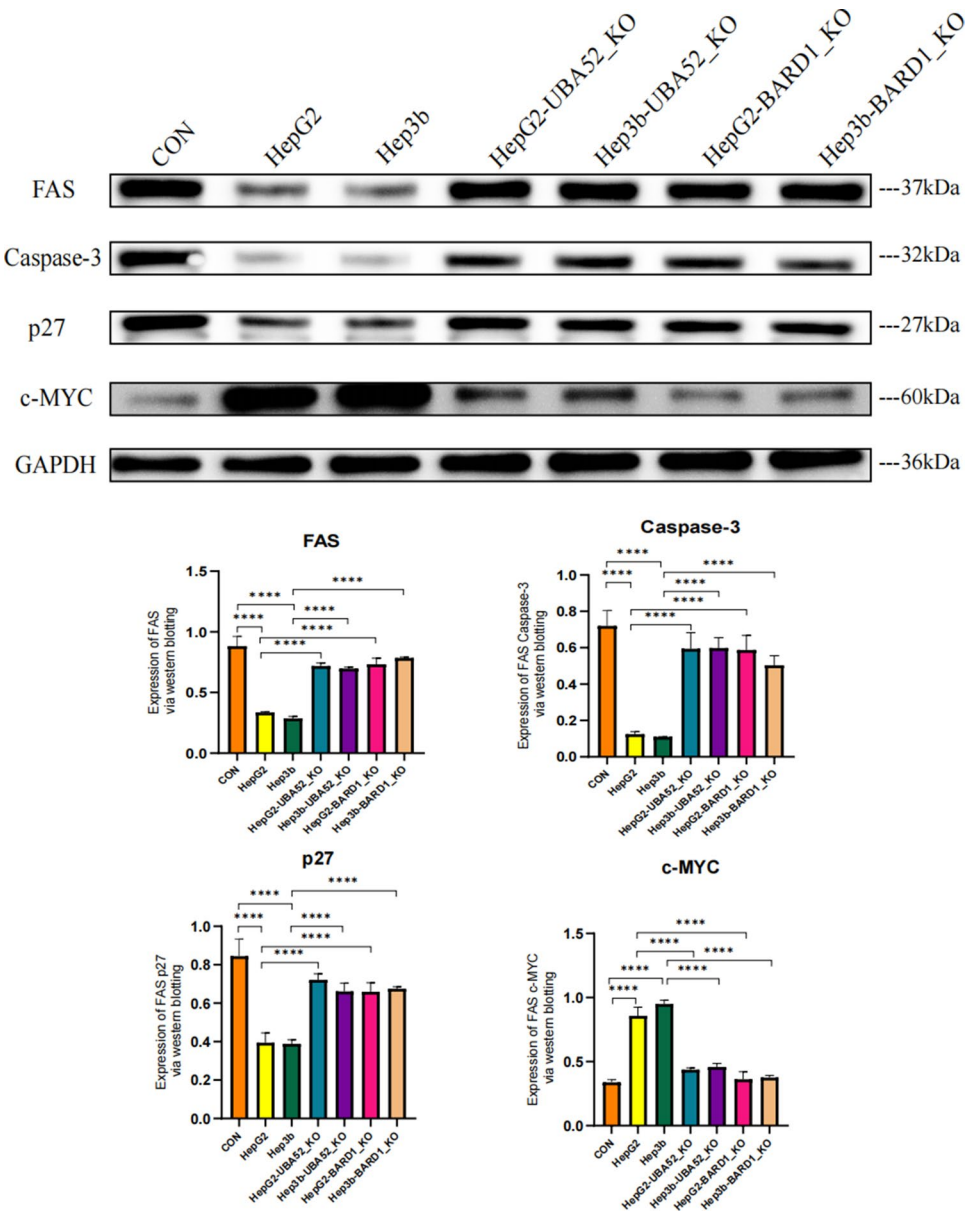

Fig. 15 RT-qPCR analysis of BARD1 and UBA52 expression in liver cell lines. Relative mRNA expression of BARD1 (left) and UBA52 (right) in normal liver cells (CON), HepG2 human liver cancer cells, Hep3b human liver cancer cells, and PI3 K inhibitor-treated HepG2 and Hep3b cells. Data are shown as mean ± SD from at least three independent experiments. Significant differences were determined by t-test (*$p < 0.05$). BARD1 and UBA52 expression was higher in HepG2 and Hep3b cells compared to the CON group ($p < 0.05$), and PI3 K inhibition reduced their expression in treated cells ($p < 0.05$)

homeostasis, and its abnormal expression may lead to cell cycle disorder and uncontrolled proliferation of tumor cells. Substances released after mast cell activation may promote the proliferation of tumor cells, and this promoting effect may promote the development of HCC together with abnormal expression of UBA52. On the other hand, UBA52 may indirectly regulate the activation of mast cells by affecting some signaling pathways, forming a complex feedback loop, and further affecting the occurrence and development of tumors. BARD1 is a tumor suppressor gene, which interacts with BRCA1 to participate in DNA damage repair and other processes. The relatively higher mast cell activation in HCC samples may have an impact on BARD1 function. The inflammatory mediators released by mast cells may cause DNA damage. If BARD1 is normally expressed, it can initiate DNA damage repair mechanism to maintain genomic stability and inhibit tumor development. However, the loss or dysfunction of BARD1 expression cannot effectively repair the damaged DNA, which may lead to genomic instability of tumor cells and promote the development of HCC. At the same time, mast cell activation may affect the expression and function of BARD1 by regulating immune cell infiltration and cytokine secretion in the tumor microenvironment, forming a complex network relationship and jointly affecting the

progression of HCC. There are complex interactions between them, which jointly affect the occurrence and development of HCC and the formation of tumor microenvironment.

There is a lack of novel biomarkers for poor prognosis of HCC, and studies have shown that portal vein and hepatic artery coefficients predict overall survival and recurrence-free survival in patients with HCC after hepatectomy [35]. Hypoxia stress at high altitude plays a role in hepatocellular carcinoma [36]. Tumor-associated lymphatic vessel density is a postoperative prognostic biomarker of hepatobiliary cancers [37]. In this study, we used bioinformatics analysis and cell experiments to verify the high expression of UBA52 and BARD1 in HCC. We found that both may promote the proliferation, survival, and metastasis of HCC cells by regulating the PI3 K/AKT signaling pathway, apoptosis factors, and the cell cycle. Although this study provides new clues to the molecular mechanisms of HCC, there are still some limitations. Gene overexpression and knockout experiments have not been performed, and direct functional verification is lacking. In addition, the analysis results of this study are based on public datasets and need to be further confirmed in combination with animal models and clinical samples to determine the biological significance of UBA52 and BARD1. Future studies should further reveal their molecular mechanisms through in vivo and in vitro experiments to provide a more comprehensive basis for the diagnosis and treatment of HCC.

5 Conclusion

In summary, UBA52 and BARD1 are highly expressed in HCC, and their high expression is closely related to poor prognosis in patients with liver cancer. UBA52 and BARD1 may be involved in the occurrence and development of liver cancer by regulating the proliferation, migration, and drug resistance of HCC cells. Future research can further explore the potential of these two genes as therapeutic targets for liver cancer, providing new ideas for the early diagnosis and targeted treatment of HCC.

Acknowledgements None.

Author contributions Chenrui Yang performed experiments mentioned in the paper, contributed to the work concept and design of the paper research, Yanzhong Zhang collected data, Yajuan Liu and Xiaoyong Wu made statistical analysis of data, Fangyuan Sun drafted the manuscript. Chenrui Yang and Yanzhong Zhang revised the main content of the manuscript. All authors read and agree on the manuscript.

Funding Project number: WSJK2024MS223, Hainan Joint General Project of Health Science and Technology Innovation.

Data availability The datasets generated during and/or analyzed during the current study are available from the corresponding author on reasonable request.

Declarations

Ethics approval and consent to participate This study was approved by the ethics committee of Danzhou People's Hospital (Danzhou People's Hospital Medical Group). The research was carried out following the guidelines of the ethics committee listed in the ethics statement.

Competing interests The authors declare no competing interests.

References

1. Bray F, Laversanne M, Sung H, et al. Global cancer statistics 2022: GLOBOCAN estimates of incidence and mortality worldwide for 36 cancers in 185 countries. CA Cancer J Clin. 2024;74(3):229–63.
2. Yang JD, Hainaut P, Gores GJ, Amadou A, Plymoth A, Roberts LR. A global view of hepatocellular carcinoma: trends, risk, prevention and management. Nat Rev Gastroenterol Hepatol. 2019;16(10):589–604.

3. Vogel A, Meyer T, Sapisochin G, Salem R, Saborowski A. Hepatocellular carcinoma. Lancet. 2022;400(10360):1345–62.
4. Ally A, Balasundaram M, Carlsen R, et al. Comprehensive and integrative genomic characterization of hepatocellular carcinoma. Cell. 2017;169(7):1327-1341.e23.
5. Sun Y, Wu P, Zhang Z, et al. Integrated multi-omics profiling to dissect the spatiotemporal evolution of metastatic hepatocellular carcinoma. Cancer Cell. 2024;42(1):135-156.e17.
6. Abusaliya A, Bhosale PB, Kim HH, et al. Investigation of prunetrin induced G2/M cell cycle arrest and apoptosis via Akt/mTOR/MAPK pathways in hepatocellular carcinoma cells. Biomed Pharmacother. 2024;174: 116483.
7. Dantzer C, Dif L, Vaché J, Basbous S, Billottet C, Moreau V. Specific features of ß-catenin-mutated hepatocellular carcinomas. Br J Cancer. 2024;131(12):1871–80.
8. Kitao A, Matsui O, Zhang Y, et al. Dynamic CT and gadoxetic acid-enhanced MRI characteristics of P53-mutated hepatocellular carcinoma. Radiology. 2022;306(2): e220531.
9. Wu Y, Wang J, Zhao J, et al. LTR retrotransposon-derived LncRNA LINC01446 promotes hepatocellular carcinoma progression and angiogenesis by regulating the SRPK2/SRSF1/VEGF axis. Cancer Lett. 2024;598: 217088.
10. Chen D, Liu J, Zang L, et al. Integrated machine learning and bioinformatic analyses constructed a novel stemness-related classifier to predict prognosis and immunotherapy responses for hepatocellular carcinoma patients. Int J Biol Sci. 2022;18(1):360–73.
11. Zhang Z, Chen S, Jun S, et al. MLKL-USP7-UBA52 signaling is indispensable for autophagy in brain through maintaining ubiquitin homeostasis. Autophagy. 2025. https://doi.org/10.1080/15548627.2024.2395727.
12. Wu D, Huang H, Chen T, et al. The BRCA1/BARD1 complex recognizes pre-ribosomal RNA to facilitate homologous recombination. Cell Discov. 2023;9(1):99.
13. Forner A, Reig M, Bruix J. Hepatocellular carcinoma. Lancet. 2018;391(10127):1301–14.
14. Chan A, Kow A, Hibi T, Di Benedetto F, Serrablo A. Liver resection in cirrhotic liver: are there any limits. Liver Transplant Hepatobil Surg Int J Surg. 2020;82:109–14.
15. Yu Z, Keskinocak P, Magliocca JF, Romero R, Sokol J. Split or whole liver transplantation? Utilization and posttransplant survival. Hepatol Commun. 2023. https://doi.org/10.1097/HC9.0000000000000225.
16. Xia S, Pan Y, Liang Y, Xu J, Cai X. The microenvironmental and metabolic aspects of sorafenib resistance in hepatocellular carcinoma. EBioMedicine. 2020. https://doi.org/10.1016/j.ebiom.2019.102610.
17. Xu C, Xu Z, Zhang Y, Evert M, Calvisi DF, Chen X. β-Catenin signaling in hepatocellular carcinoma. J Clin Investig. 2022. https://doi.org/10.1172/JCI154515.
18. Sun B, Ding P, Song Y, et al. FDX1 downregulation activates mitophagy and the PI3K/AKT signaling pathway to promote hepatocellular carcinoma progression by inducing ROS production. Redox Biol. 2024;75: 103302.
19. Chen J, Gingold JA, Su X. Immunomodulatory TGF-β signaling in hepatocellular carcinoma. Trends Mol Med. 2019;25(11):1010–23.
20. Cai N, Cheng K, Ma Y, et al. Targeting MMP9 in CTNNB1 mutant hepatocellular carcinoma restores CD8+ T cell-mediated antitumour immunity and improves anti-PD-1 efficacy. Gut. 2024;73(6):985.
21. Liang B, Wang H, Qiao Y, et al. Differential requirement of Hippo cascade during CTNNB1 or AXIN1 mutation-driven hepatocarcinogenesis. Hepatology. 2023. https://doi.org/10.1002/hep.32693.
22. Yu J, Ling S, Hong J, et al. TP53/mTORC1-mediated bidirectional regulation of PD-L1 modulates immune evasion in hepatocellular carcinoma. J ImmunoTherapy Cancer. 2023;11(11): e007479.
23. Baker RT, Board PG. The human ubiquitin-52 amino acid fusion protein gene shares several structural features with mammalian ribosomal protein genes. Nucleic Acids Res. 1991;19(5):1035–40.
24. Yao Y, Xu T, Li X, et al. Selenoprotein S maintains intestinal homeostasis in ulcerative colitis by inhibiting necroptosis of colonic epithelial cells through modulation of macrophage polarization. Theranostics. 2024;14(15):5903–25.
25. Mughees M, Wajid S, Samim M. Cytotoxic potential of Artemisia absinthium extract loaded polymeric nanoparticles against breast cancer cells: Insight into the protein targets. Int J Pharm. 2020;586: 119583.
26. Zhou Q, Hou Z, Zuo S, et al. LUCAT1 promotes colorectal cancer tumorigenesis by targeting the ribosomal protein L40-MDM2-p53 pathway through binding with 52. Cancer Sci. 2019;110(4):1194–207.
27. Setayesh SM, Ndacayisaba LJ, Rappard KE, et al. Targeted single-cell proteomic analysis identifies new liquid biopsy biomarkers associated with multiple myeloma. NPJ Precis Oncol. 2023;7(1):95.
28. Tong L, Zheng X, Wang T, et al. Inhibition of UBA52 induces autophagy via EMC6 to suppress hepatocellular carcinoma tumorigenesis and progression. J Cell Mol Med. 2024;28(6): e18164.
29. Russi M, Marson D, Fermeglia A, et al. The fellowship of the RING: BRCA1, its partner BARD1 and their liaison in DNA repair and cancer. Pharmacol Ther. 2022;232: 108009.
30. Qiu L, Xu W, Lu X, et al. The HDAC6-RNF168 axis regulates H2A/H2A.X ubiquitination to enable double-strand break repair. Nucleic Acids Res. 2023;51(17):9166–82.
31. Ceppi I, Dello Stritto MR, Mütze M, et al. Mechanism of BRCA1–BARD1 function in DNA end resection and DNA protection. Nature. 2024;634(8033):492–500.
32. Witus SR, Zhao W, Brzovic PS, Klevit RE. BRCA1/BARD1 is a nucleosome reader and writer. Trends Biochem Sci. 2022;47(7):582–95.
33. Randall MP, Egolf LE, Vaksman Z, et al. BARD1 germline variants induce haploinsufficiency and DNA repair defects in neuroblastoma. JNCI J Natl Cancer Inst. 2024;116(1):138–48.
34. Jain A, McCoy M, Coats C, et al. HuR plays a role in double-strand break repair in pancreatic cancer cells and regulates functional BRCA1-associated-ring-domain-1(BARD1) isoforms. Cancers (Basel). 2022. https://doi.org/10.3390/cancers14071848.
35. Li YK, Wu S, Wu YS, Zhang WH, Wang Y, Li YH, et al. Portal venous and hepatic arterial coefficients predict post-hepatectomy overall and recurrence-free survival in patients with hepatocellular carcinoma: a retrospective study. J Hepatocell Carcinoma. 2024;11:1389–402. https://doi.org/10.2147/JHC.S462168.
36. Liang Y, Li L, Liu B, Gao J, Chen X, Li J, et al. Research advances in the roles of high-altitude hypoxic stress in hepatocellular carcinoma. Sichuan Da Xue Xue Bao Yi Xue Ban. 2024;55(6):1436–45. https://doi.org/10.12182/20241160605.

37. Li J, Liang YB, Wang QB, Li YK, Chen XM, Luo WL, et al. Tumor-associated lymphatic vessel density is a postoperative prognostic biomarker of hepatobiliary cancers: a systematic review and meta-analysis. Front Immunol. 2024;15:1519999. https://doi.org/10.3389/fimmu.2024.1519999.